Macroscopic and microscopic electrical characterizations of high-k ZrO_2 and $ZrO_2/Al_2O_3/ZrO_2$ metal-insulator-metal structures

Dominik Martin[a] and Matthias Grube
Namlab gGmbH, 01187 Dresden, Germany

Wenke Weinreich, Johannes Müller, and Lutz Wilde
Fraunhofer CNT, 01099 Dresden, Germany

Elke Erben, Walter M. Weber, Johannes Heitmann,[b] and Uwe Schröder[b]
Namlab gGmbH, 01187 Dresden, Germany

Thomas Mikolajick
Namlab gGmbH, 01187 Dresden, Germany and Chair of Nanoelectronic Materials, 01062 Dresden, Germany

Henning Riechert
Paul-Drude-Institut für Festkörperelektronik, 10117 Berlin, Germany

(Received 11 August 2010; accepted 8 November 2010; published 14 January 2011)

In order for sub-10 nm thin films of ZrO_2 to have a dielectric constant larger than 30 they need to be crystalline. This is done by either depositing the layer at higher temperatures or by a postdeposition annealing step. Both methods induce high leakage currents in ZrO_2 based dielectrics. In order to understand the leakage a thickness series of ultrathin ZrO_2 and nanolaminate $ZrO_2/Al_2O_3/ZrO_2$ (ZAZ) films, deposited by atomic layer deposition, was investigated. After deposition these films were subjected to different rapid thermal annealing (RTA) processes. Grazing incidence x-ray diffraction and transmission electron microscopy yield that the crystallization of ZrO_2 during deposition is dependent on film thickness and on the presence of an Al_2O_3 sublayer. Moreover, the incorporation of Al_2O_3 prevents crystallites from spanning across the entire film during RTA. *C-V* and *I-V* spectroscopies show that after a 650 °C RTA in N_2 the capacitance equivalent oxide thickness of 10 nm ZAZ films is reduced to 1.0 nm while maintaining low leakage currents of 3.2×10^{-8} A/cm^2 at 1 V. Conductive atomic force microscopy studies yield that currents are not associated with significant morphological features in amorphous layers. However, after crystallization, the currents at crystallite grain boundaries are increased in ZrO_2 and ZAZ films.

© *2011 American Vacuum Society.*

[DOI: 10.1116/1.3523397]

I. INTRODUCTION

Future dynamic random access memory (DRAM) and logic technology nodes require insulating materials with high dielectric constants. These are very difficult to achieve with purely amorphous thin films since higher dielectric constants are obtained in crystalline phases. To achieve a k-value larger than 30 in thin ZrO_2 films it is necessary to obtain the tetragonal crystalline phase. This is done by either depositing the layer at high temperatures or by a postdeposition annealing step. Both methods induce high leakage currents. To reduce these small amounts of Al_2O_3 can be incorporated in the center of a ZrO_2 film, forming a $ZrO_2/Al_2O_3/ZrO_2$ (ZAZ) film. ZrO_2 films have been shown to fulfill the requirements of the 50 nm DRAM technology node.[1,2] Incorporation of very small amounts of Al_2O_3 into ZrO_2 reduces leakage while maintaining a sufficiently high dielectric constant.[3–6] A deeper understanding of the mesoscopic mechanisms involved is essential for future materials engineering. This work is a comparative study of thickness series of ultrathin ZrO_2 and ZAZ films, deposited by atomic layer deposition (ALD) carried out in order to gain a deeper understanding of leakage mechanisms and the effect of Al incorporation in ultrathin dielectric films. After deposition these films were subjected to different rapid thermal annealing (RTA) processes and characterized by grazing incidence x-ray diffraction (GIXRD), x-ray reflectometry (XRR), transmission electron microscopy (TEM), *I-V* and *C-V* spectroscopies, and

TABLE I. List of sample and deposition parameters. For simplicity, films are addressed by their target thickness. The cycle sequence was TEMAZ for ZrO_2 and TEMAZ/TMA/TEMAZ for ZAZ. The oxygen precursor was ozone and the deposition temperature was 270 °C.

Name	Material	Target thickness (nm)	Cycle sequence
Z6	ZrO_2	6	64
Z8	ZrO_2	8	86
Z10	ZrO_2	10	110
ZAZ6	ZAZ	6	32/2/28
ZAZ8	ZAZ	8	42/2/41
ZAZ10	ZAZ	10	53/2/53

[a] Electronic mail: martin@namlab.com
[b] Formerly with Qimonda Dresden GmbH & Co OHG, 01099 Dresden, Germany.

Author complimentary copy. Redistribution subject to AIP license or copyright, see http://jvb.aip.org/jvb/copyright.jsp

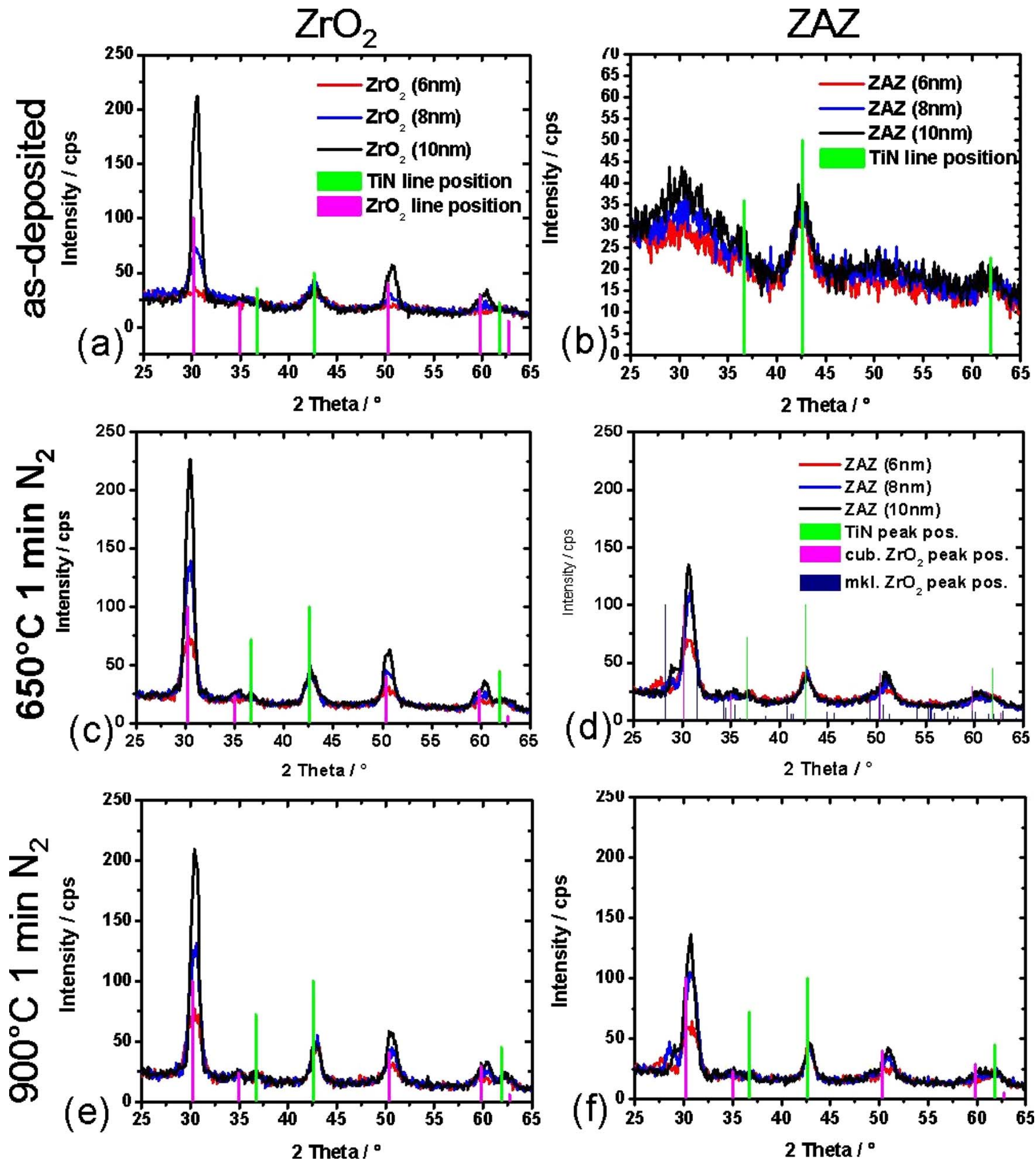

FIG. 1. (Color online) GIXRD graphs of as-deposited [(a) and (b)] films and of films that have been subjected to a 1 min 650 °C N_2 [(c) and (d)] or 900 °C N_2 [(e) and (f)] RTA process. (a), (c), and (e) are of ZrO_2 and (b), (d), and (f) are of ZAZ films. (a) clearly yields enhanced crystallization with increased layer thickness of ZrO_2. Al incorporation has suppressed crystallization during deposition (b). ZAZ films that are annealed show a satellite peak to the 30.5° ZrO_2 peak [(d) and (f)]. The satellite peak is shifted toward the main peak as film thickness increases.

conductive atomic force microscopy (CAFM). CAFM has already been used to identify nanoscale crystallites as the origin of high leakage currents.[7–11]

II. EXPERIMENT

A 10 nm thick TiN bottom electrode (BE) was deposited by physical vapor deposition onto a highly *n*-doped silicon substrate. The dielectric layers where deposited by ALD in a commercial ALD system. The precursors were tetrakis[ethylmethylamino]zirconium (TEMAZ), trimethylaluminum (TMA), and ozone for Zr, Al, and oxygen, respectively. Two types of films were deposited, pure ZrO_2 and ZAZ stacks, all at 270 °C. With only 2 cycles of Al included in the center of the film it can well be assumed that the Al_2O_3 layer is not completely closed. The ZrO_2 layers and ZAZ stacks were targeted at 6, 8, and 10 nm. Deposition parameters are summarized in Table I. Two different RTA processes were carried out, 1 min at 650 °C or 1 min at 900 °C process, both in nitrogen atmosphere. The top electrodes (TEs) for electrical characterization consisting of a 10 nm Ti adhesion layer followed by 200 nm of Al were deposited by electron beam evaporation (Ti) and thermal evaporation (Al) completing the metal-insulator-metal (MIM) structure. The TE sizes were 6.25×10^{-5}, 2.25×10^{-5}, and 1.40×10^{-5} cm^2. To reduce er-

Author complimentary copy. Redistribution subject to AIP license or copyright, see http://jvb.aip.org/jvb/copyright.jsp

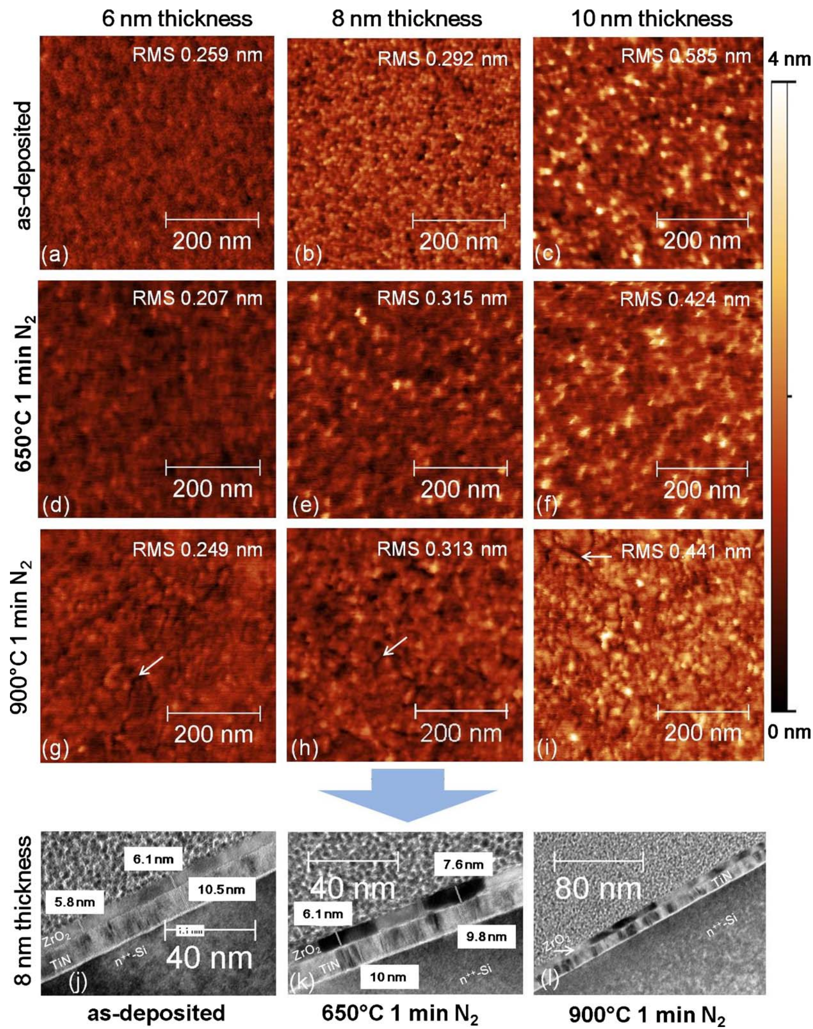

FIG. 2. (Color online) AFM morphology maps of the as-deposited and annealed ZrO_2. (a)–(c) are as deposited, (d)–(f) were subjected to a 1 min 650 °C RTA in N_2, and (g)–(i) were subjected to a 1 min 900 °C RTA in N_2. Layer thickness is 6 nm (Z6) for (a), (d), and (g); 8 nm (Z8) for (b), (e), and (h); and 10 nm (Z10) for (c), (f), and (i). Increased layer thickness shows enhanced surface features in the form of hillocks appearing considerably brighter. Increased annealing temperature induces a network of interconnected trenches. The white arrow in images (g)–(i) marks such representative trenches. TEM micrographs of the 8 nm thick ZrO_2 films as deposited (j), after 650 °C RTP (k), and 900 °C RTP (l), and increase in crystallite grain size is visible from (j) to (l). Note the different scale bars.

rors the size of each individual TE was measured and used for the current density calculation. Physical characterization was carried out by GIXRD, XRR, TEM, and AFM. Film thickness was determined by ellipsometry, XRR, and TEM. Electrical characterization was done by combining CAFM, and *C-V* and *I-V* spectroscopies. To ensure the reliability of the *CV* measurements a parallel circuit model was used and all measurements where the dissipation factor exceeded 0.1 were considered as nonreliable and disregarded. The delay time used to exclude dielectric relaxation from measurement was 2 s, and the frequency for the *CV* measurements was 100 kHz. CAFM measurements were done by operating an AFM in contact using a conductive Pt coated probe.[8,10,11] During measurement the AFM tip was grounded and the sample was set to negative potential resulting in substrate electron injection. The cantilever deflection was constantly monitored on a third channel, ensuring constant pressure between tip and sample. The AFM (Veeco DI Dimension 3100) was equipped with a preamplifier with a noise level <100 fA (rms). A high resolution topography map was first taken of each sample at 0 V. At higher bias voltages resolution decreases. When bias voltage was increased in successive images, topography was always closely monitored to ensure that the scanned area was not shifted unnoticed.

III. RESULTS AND DISCUSSION

A. Structural characterization

First the film structure was studied. Figure 1(a) depicts GIXRD studies of the as-deposited ZrO_2, which shows crystallization for layer thicknesses starting at 8 nm in sample Z8. GIXRD yields that at film thicknesses exceeding 6 nm ZrO_2 crystallites form during deposition. Figure 1(b) shows that the incorporation of 2 cycles of Al sufficiently suppresses crystallization during growth in even thicker films. Figures 1(c) and 1(e) simply demonstrate that ZrO_2 is crystalline after the 650 and 900 °C RTAs. In contrast, ZAZ exhibits in Figs. 1(d) and 1(f) an extra peak just left of the large peak at approximately $2\cdot\theta=30°$ associated with cubic and tetragonal ZrO_2. This satellite is shifted toward the ZrO_2 peak with increasing film thickness. The origin of this peak is believed to be related to strained crystallites.

The effect on morphology and the extension of the crystallites within the dielectric are studied by AFM and TEM next. Figures 2(a)–2(i) depict AFM topography maps of the ZrO_2 layers. The number and height of the bright "hillock" features and surface roughness increase with film thickness. After the 650 °C N_2 RTA surface roughness decreases for all except the 8 nm film. After the 900 °C N_2 RTA the surface

Author complimentary copy. Redistribution subject to AIP license or copyright, see http://jvb.aip.org/jvb/copyright.jsp

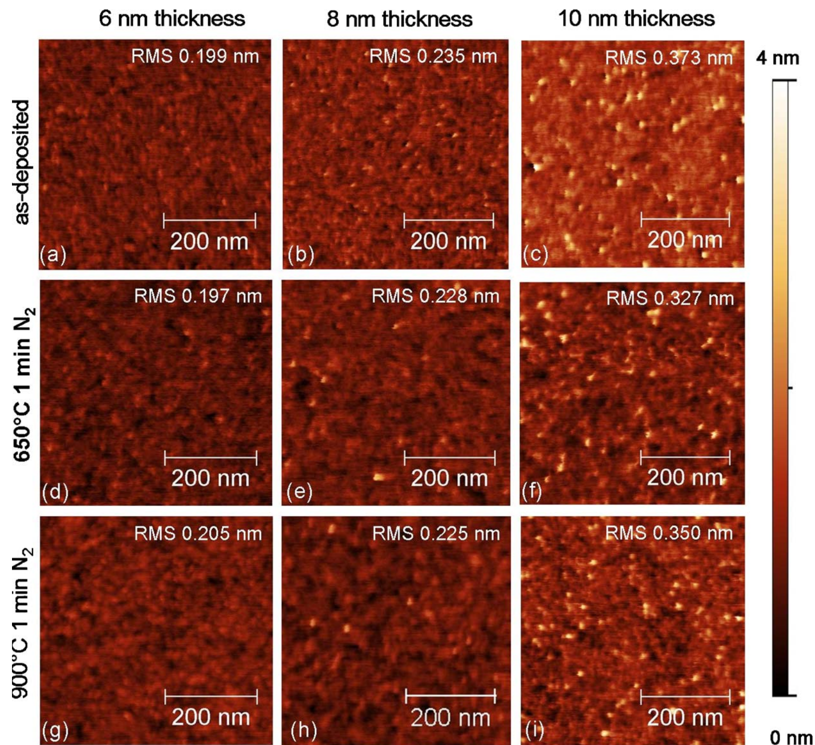

FIG. 3. (Color online) AFM morphology maps of the as-deposited and annealed ZAZ. (a)–(c) are as deposited, (d)–(f) were subjected to a 1 min 650 °C RTA process in N_2, and (g)–(i) were subjected to a 1 min 900 °C RTA process in N_2. Layer thickness is 6 nm (ZAZ6) for (a), (d), and (g); 8 nm (ZAZ8) for (b), (e), and (h); and 10 nm (ZAZ10) for (c), (f), and (i). Increased layer thickness induces pronounced surface features in the form of hillocks. Increased annealing temperature induces enhanced surface features only for the 8 and 10 nm thick films.

roughness increases again. Moreover, all ZrO_2 samples exhibit a network of interconnected trenches separating large areas. The TEM micrographs shown in Figs. 2(j)–2(l) demonstrate for Z8 the evolution from small, ≈5 nm wide, crystallites formed during growth (j), to larger, ≈20 nm wide, crystallites after 650 °C RTA (k), to even larger, ≈50 nm wide, ones after 900 °C RTA (l). This is in agreement with the network of trenches visible in AFM topography maps formed after the 900 °C RTA. An interfacial layer can be seen between the BE and the ZrO_2. This layer does not contribute to surface roughness.

Figure 3 shows AFM topography maps of the ZAZ films. The influence of layer thickness can be seen from left to right. Hillocklike features can be seen in (c), (f), and (i), the thickest films. The effect of annealing temperature is not as pronounced as in ZrO_2. The two thicker films in Fig. 3(h)(i) develop surface features analog to Fig. 2(h)(i) but far less pronounced. A small change in surface roughness is observed prior and posterior to RTA in the 6 and 8 nm ZAZ films, ZAZ6 and ZAZ8. The 10 nm ZAZ film ZAZ10 gets smoother after the 650 °C annealing and rougher after the 900 °C annealing. Comparison of surface roughness in Fig. 4 yields that surface roughness increases more sharply with film thickness for ZrO_2 than for ZAZ. The increase in surface roughness with film thickness is evident for both types of films; as-deposited ZrO_2, however, is rougher than ZAZ stacks.

Figure 5 depicts a detailed TEM analysis of the as-deposited 10 nm ZAZ films (ZAZ10) (a) before and (b) after RTA. In Fig. 5(a) a fine line is observed in the center of the ZrO_2 layer. Although energy-filtered TEM does not resolve Al at this location, this line can be associated with the $A1_2O_3$. It can be assumed that this is the location of the $A1_2O_3$. It is also shown that crystallites end abruptly at this location. The deposition of Al_2O_3 interrupts crystal growth. An interfacial layer between BE and dielectric is also observed, as already described by Weinreich *et al.*[12] In Fig. 5(b) it is observed that after 650 °C RTA separate crystallites arise in the layer. Together with the GIXRD analysis this shows that already 2 cycles of Al interrupt crystallization during deposition due to a different crystallization behavior being favorable after Al_2O_3 deposition.

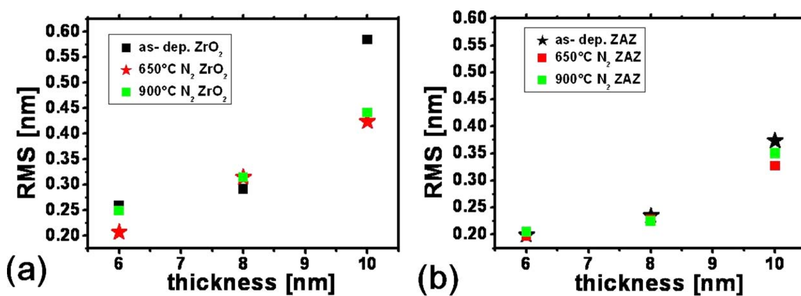

FIG. 4. (Color online) Comparison of AFM surface roughness change of (a) ZrO_2 and (b) ZAZ (b) increasing film thickness.

Author complimentary copy. Redistribution subject to AIP license or copyright, see http://jvb.aip.org/jvb/copyright.jsp

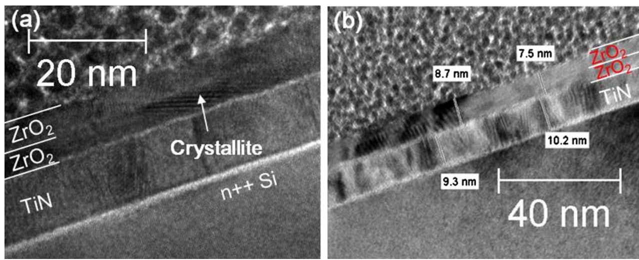

FIG. 5. (Color online) ZAZ10: (a) TEM micrograph of the 10 nm as-deposited ZAZ stack. It depicts the abrupt termination of a crystallite in the middle of the layer. It can be well assumed that this is the location of the Al. (b) After a RTP for 1 min at 650 °C in N_2 crystallites extend through the entire layer. Note the different scale bars.

B. Electrical characterization

The MIM structures with Ti/Al TEs are investigated by *IV* and *CV* measurements. The results of these are summarized in Fig. 6. In the ZrO_2 thickness series the capacitance equivalent thickness (CET) values for films thicker than 6 nm are not proportional to film thickness. Combining this information with GIXRD and TEM data, this suggests that these films are of different crystallinity and therefore exhibit different dielectric constants. For ZrO_2 the 650 °C RTA effectively lowers the CET but leakage increases from 2.3×10^{-9} to 5.9×10^{-4} A/cm^2. The CET is now proportional with film thickness. Structural analysis confirms the crystalline nature of all three ZrO_2 films. For ZrO_2 a *k*-value of 47 can be obtained out of the linear fit, which is close to the theoretical value of 46.6 for the tetragonal phase.[13] This fit crosses the ordinate above 0 nm; this is due to an interfacial TiON layer also visible in TEM images in Figs. 5 and 2(j)–2(l).[12] After annealing at 900 °C leakage currents increase dramatically, and determination of capacitance is no longer possible.

The results obtained for as-deposited ZAZ films show that incorporation of Al_2O_3 into the ZrO_2 lowers capacitance. This effect increases with film thickness. Since this film thickness dependent crystallization is suppressed in ZAZ films the crystal structure is similar within the series. Thus, the CET values have a stronger linearity to the layer thickness. The leakage current of the ZAZ films is slightly lower than for the corresponding ZrO_2 films, except for the 10 nm thick film Z10. After RTA the effect of Al_2O_3 incorporation is more evident. The 650 °C RTA induces higher surface roughness in topography. TEM analysis yields that crystallite grain sizes increase after this treatment. The incorporation of Al_2O_3 prevents the formation of crystallites spanning the entire dielectric layer. Using the example of the 10 nm ZrO_2 and ZAZ films, Z10 and ZAZ10, Fig. 6(b) shows how different RTAs affect the electrical performance of dielectric layers. The blue arrow indicates how Z10 degrades during 650 °C RTA, whereas the violet arrow demonstrates that this treatment applied to ZAZ10 results in a lower CET of 1 nm while maintaining leakage current density at 3.2×10^{-8} A/cm^2, satisfying the ITRS DRAM requirements. The green arrow shows the consequence of a 900 °C RTA on ZAZ10. After RTA the 10 nm ZAZ film has a CET of 0.8 nm and a leakage current density of 1.1×10^{-6} A/cm^2 at 1 V. In both cases CET was significantly lowered while maintaining low leakage currents. Moreover, the leakage current versus CET for the 6 (Z6) and 8 nm (Z8) ZrO_2 and the 6 nm (ZAZ6) films are all allocated around CET=0.6 nm and 1×10^{-3} A/cm^2.

C. Mesoscopic electrical characterization

CAFM provides detailed topographical information correlated with conductivity information. Since the thickest samples show the highest number of topographical features and changes after RTA, these samples are compared by CAFM. In Fig. 7 the topography map (a) of 10 nm thick as-deposited ZrO_2 (Z10) is compared to the current (b) measured in that area at −5.6 V. The surface is rough. The hillocks cannot be correlated with high currents. Current appears

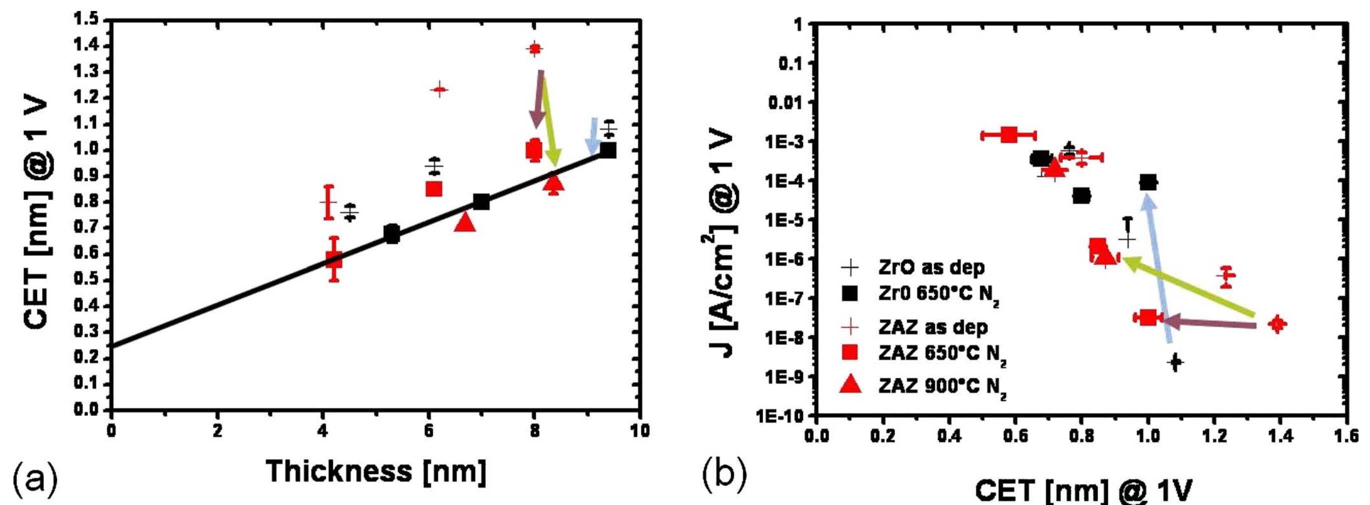

FIG. 6. (Color online) (a) CET at 1 V of all measurable samples plotted over layer thickness. The linear fit for ZrO_2 annealed at 650 °C yields a *k*-value of 47. (b) Leakage current at 1 V plotted over CET at 1 V. The arrows indicate the impact of a 650 °C RTAs on 10 nm ZrO_2 and 10 nm ZAZ.

Author complimentary copy. Redistribution subject to AIP license or copyright, see http://jvb.aip.org/jvb/copyright.jsp

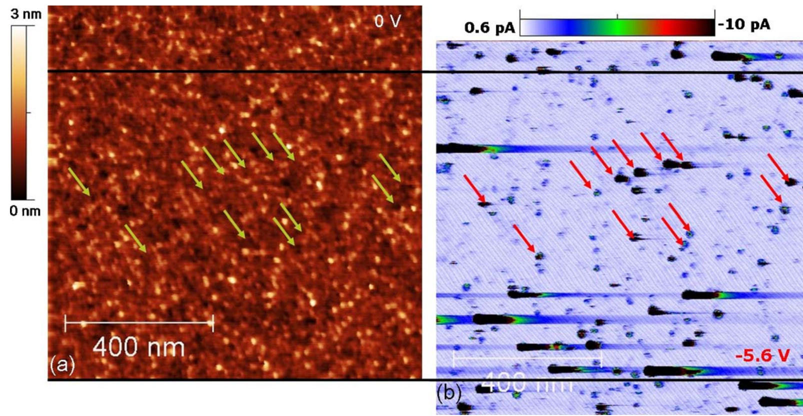

FIG. 7. (Color online) Z10: (a) CAFM topography map of the as-deposited 10 nm ZrO_2 film taken at 0 V where spatial resolution is best. The surface is rough exhibiting hillocklike features. (b) CAFM current map taken at −5.6 V substrate injection. The false color bar is linear. The offset between (a) and (b) is due to "piezocreep." High currents are correlated with depressions in the surface.

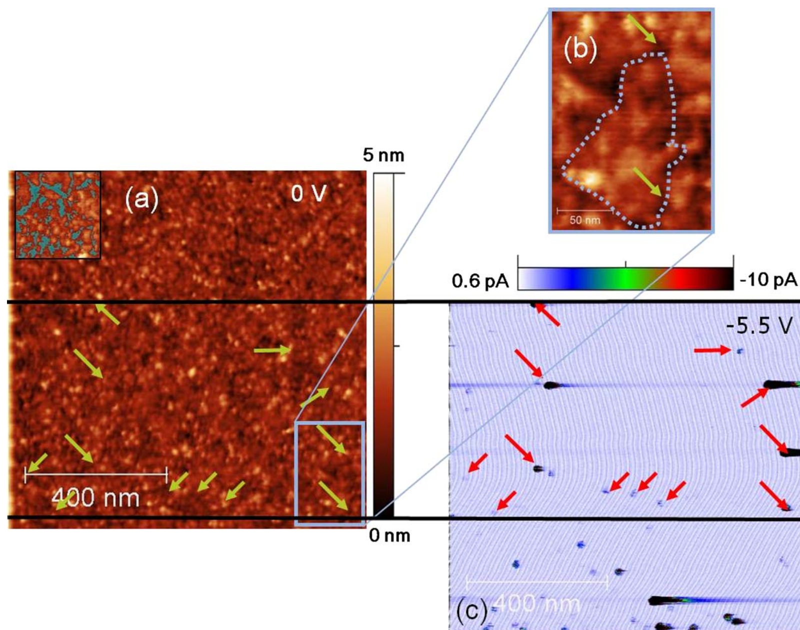

FIG. 8. (Color online) Z10: after RTA (a) CAFM topography map of the 10 nm ZrO_2, film subjected to 900 °C in N_2, taken at 0 V. The surface is rough exhibiting hillocklike features and interconnected trenches; see (b). The inset in (a) shows this in a 74.1% threshold analysis (Ref. 16). These separate large areas of the surface, (c) CAFM current map taken at −5.5 V (substrate injection). The false color bar is linear. High currents are correlated with trenches separating grains.

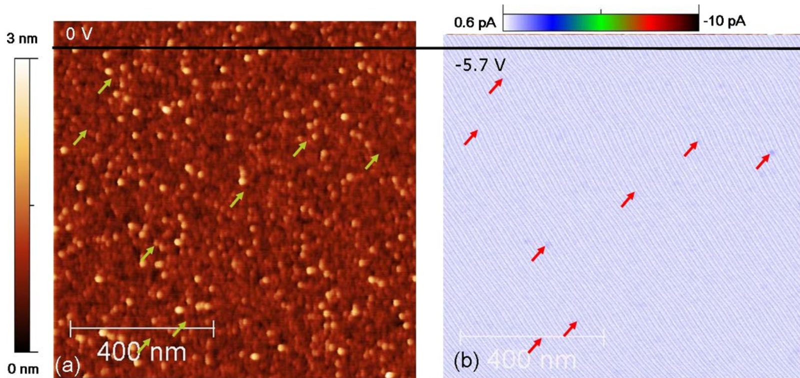

FIG. 9. (Color online) ZAZ10: (a) CAFM topography map of the as-deposited 10 nm ZAZ film taken at 0 V. Hillocks are visible, (b) CAFM current map taken at −5.7 V (substrate injection). The false color bar is linear. Few low current spots are barely measurable and cannot be associated with distinct morphological features.

Author complimentary copy. Redistribution subject to AIP license or copyright, see http://jvb.aip.org/jvb/copyright.jsp

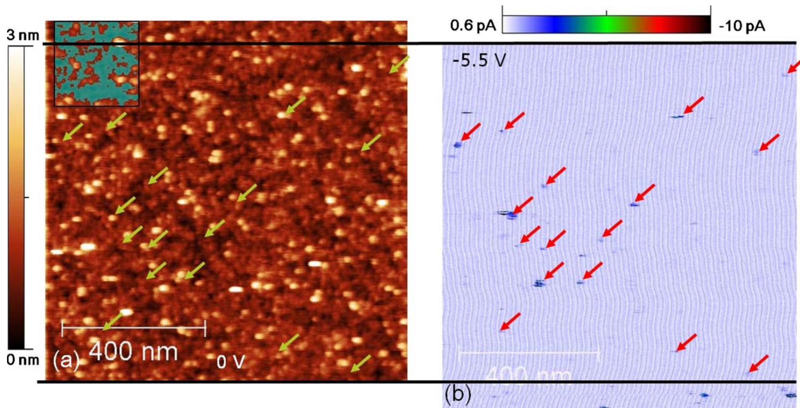

Fig. 10. (Color online) ZAZ10 after RTA: (a) CAFM topography map of the 10 nm ZAZ, film subjected to 900 °C in N_2, taken at 0 V. The hillocklike features prevail through RTA and only an incipient underlying network of trenches is visible. The inset in (a) shows this in a 74.1% threshold analysis (Ref. 16). (b) CAFM current map taken at −5.5 V (substrate injection). The false color bar is linear. Compared to Fig. 9 more current spots of higher current are measured.

in the form of "hot spots" with a diameter of between 15 and 25 nm. These are extremely local dielectric breakdowns induced by the high electric field under the AFM probe. For comparison, the locations of these spots are marked with a red arrow in the current map, and with a green arrow in the topology map. These spots are located at depressions in topography. The high number of hot spots predicts the increased leakage currents observed in macroscopic *I-V* measurements after RTA.

In Fig. 8 the topography map (a) of 10 nm thick ZrO_2 (Z10), annealed at 900 °C, is compared to the current map (c) at −5.5 V. In addition to hillocks interconnected trenches are observed. These are not visible in the as-deposited sample. The inset of Fig. 8(b) shows how these trenches separate an entire area from the rest. It is at these trenches where current spots exceeding 10 pA in absolute value are detected. In comparison to the untreated sample the leakage spot density is lower; nevertheless macroscopic measurements show highly increased leakage currents after annealing. The difference to macroscopic measurements is due to different electric fields under the TE and the CAFM tip. Additionally, the CAFM measurements are conducted at almost six times higher bias voltage. The large TE induces a fairly homogeneous field throughout the dielectric layer in contrast to the very small CAFM probe, which induces an inhomogeneous field with extreme field enhancement close to the surface. It is assumed that CAFM induces a cascade of dielectric breakdowns associated with thermochemical bond breakage.[6,14] These are guided by existing defects.[11,15] CAFM activates defects that macroscopic measurements do not activate due to lower local electric fields. By taking the known crystallinity of the as-deposited 10 nm ZrO_2 films into account we conclude that the crystallite grain boundaries induce the large currents in the CAFM measurement. We cannot gather this information from comparing topography and current maps alone, the association with physical (TEM and GIXRD) is necessary.

In Fig. 9 the topography map (a) of a 10 nm as-deposited ZAZ10 film is compared to the current (b) measured in that area at −5.7 V. The sample surface exhibits comparable hillock structures to Z10. Some isolated recesses are visible. In Fig. 9(b) only a few current spots exceeding an absolute value of 1 pA are measured, which do not correlate with morphological features. This corresponds to the amorphous nature of the top part of the ZrO_2 film. Figure 10 compares the topography map (a) of a 10 nm ZAZ10 film annealed at 900 °C to the current map (b) measured in that area at −5.5 V. Some interconnected trenches appear, which are also at the location of currents in the current map. The number and magnitude of current spots are higher after RTA. These current spots at sites where interconnected trenches are located indicate grain boundaries.

In conclusion, these results show that keeping the films in an amorphous state during deposition is inherent for good electrical performance; while crystallization after deposition helps increase the *k*-value of the films. The electrical properties can be tuned by inserting a sublayer of Al_2O_3 into the ZrO_2. The Al_2O_3 stops crystallization during deposition by superimposing slightly different lattice parameters to the film as demonstrated by GIXRD.

IV. SUMMARY

In summary ZrO_2 and ZAZ thin films were deposited at three film thicknesses by ALD. These were subjected to two different RTA processes and then compared by GIXRD, TEM, CAFM, and *I-V* and *C-V* spectroscopies. It was shown that incorporation of only 2 cycles of Al into the center of the stack significantly improves physical and electrical properties. Al_2O_3 interrupts crystallization during deposition. In addition, it stabilizes the dielectric stack during RTA by reducing the number of grain boundaries, which were shown to be the physical defects responsible for leakage currents. While having a larger CET before RTA the ZAZ layers could be annealed at higher temperatures than ZrO_2 resulting in a lower CET and lower leakage currents, thus, demonstrating that ZAZ is a material suitable for current DRAM technology nodes. These results imply that the incorporation of a sublayer of another material can be a powerful tool for future materials design.

ACKNOWLEDGMENTS

The authors are grateful for the TEM analyses by Lutz Hillmann of Infineon Dresden GmbH. This work was supported by the German Federal Ministry of Education and Research (BMBF) under the MEGAEPOS project.

Author complimentary copy. Redistribution subject to AIP license or copyright, see http://jvb.aip.org/jvb/copyright.jsp

[1] See www. itrs.org.
[2] Kyoung-Ryul Yoon, Ki-Vin Im, Jea-Hyun Yeo, Eun-Ae Chung, Young-Sun Kim, Cha-Young Yoo, Sung-Tae Kim, U-In Chung, and Joo-Tae Moon, Extended Abstracts of the 2005 International Conference on Solid State Devices and Materials, Kobe, Japan, 2005 (unpublished), p. 188.
[3] Ho Jin Cho *et al.*, Solid-State Electron. **51**, 1529 (2007).
[4] Y. K. Park *et al.*, Dig. Tech. Pap. - Symp. VLSI Technol. **2007**, 190 (2007).
[5] Deok-Sin Kil *et al.*, Dig. Tech. Pap. - Symp. VLSI Technol. **2006**, 38 (2006).
[6] D. Zhou *et al.*, J. Appl. Phys. (accepted).
[7] W. Weinreich *et al.*, J. Vac. Sci. Technol. B **21**, 354 (2009).
[8] V. Yanev *et al.*, Appl. Phys. Lett. **92**, 252910 (2008).
[9] E. Paskaleva, M. Lemberger, A. J. Bauer, W. Weinreich, J. Heitmann, E. Erben, U. Schröder, and L. Overbeck, J. Appl. Phys. **106**, 054107 (2009).
[10] O. Bierwagen, L. Geelhaar, X. Gay, M. Piesins, B. Jobst, A. Rucki, and H. Riechert, Appl. Phys. Lett. **90**, 232901 (2007).
[11] D. Martin, M. Grube, W. M. Weber, J. Rüstig, O. Bierwagen, L. Geelhaar, and H. Riechert, Appl. Phys. Lett. **95**, 142906 (2009).
[12] W. Weinreich *et al.*, Microelectron. Eng. **86**, 1826 (2009).
[13] X. Zhao and D. Vanderbilt, Phys. Rev. B **65**, 075105 (2002).
[14] J. McPherson, J.-Y. Kim, A. Shanware, and H. Mogul, Appl. Phys. Lett. **82**, 2121 (2003).
[15] M. Grube, D. Martin, W. M. Weber, O. Bierwagen, L. Geelhaar, and H. Riechert, IEEE Proceedings of SCS2009, 2009, Paper No. SCS-NM-27.
[16] See http://gwyddion.net.

Author complimentary copy. Redistribution subject to AIP license or copyright, see http://jvb.aip.org/jvb/copyright.jsp